Active Clamped Current-Fed Full-Bridge Integrating LLC Converter with Low Current and Voltage Stress

Seung Woo Jwa, Jae Bum Lee, Yeonho Jeong, Keon-woo Kim, Gun Woo Moon
School of Electrical Engineering
KAIST
Daejeon, Republic of Korea

Jun-Ho Kim
Research & Development Division
Hyundai Motor Co.
Gyeonggi-do, Hwaseong, Republic of Korea

***Abstract*— This paper presents an active clamped current-fed full-bridge converter integrating *LLC* converter for fuel cell power system. In the proposed converter, the half-bridge *LLC* converter is integrated into the conventional active clamped current-fed full-bridge (ACCF) converter without additional active components and volume increasing. The proposed converter has a low voltage stress on the primary switches because a high step-up voltage conversion ratio can be realized with the low duty ratio *D*. In addition, due to two transformers structure, the conduction loss of main switches (S_1-S_4) is decreased by reducing of the peak current. Moreover, the turn-off and conduction losses of auxiliary switch (S_{aux}) are reduced by sinusoidal shape resonant current of the *LLC* resonant tank. To verify the performance of the proposed converter, the prototype converter with 36V-57V input and 400V/1kW output is implemented.**

Keywords*— *Fuel Cell, High step-up converter, Current-fed converter, Fuel cell power supply.

I. INTRODUCTION

With increasing concern about global warming, the demand for clean and renewable resources has been increased to reduce carbon dioxide emission. Among them, a fuel cell is one of promising clean energy source, because it directly converts the chemical energy into electric power, only producing pure water and heat. Moreover, a fuel cell has a high energy conversion efficiency. A conventional combustion based power plant typically generates electricity with low efficiency of 35.9%. Likewise, nuclear power plant generates electricity with low efficiency of 39.6%. Whereas, fuel cell can generate electricity with high efficiency of 55%. Hence, fuel cell has been considered as an excellent candidate to replace the conventional energy sources. As shown in Fig. 1, the output voltage of fuel-cell stacks is normally rather low (36V-57V) [1]. The output voltage of the fuel cell is varied widely depending on the load condition. The output voltage of the fuel cell may vary from $57V_{dc}$ at no load to $36V_{dc}$ at full load. On the other hand, the input voltage of the inverter and DC bus voltage of micro grid are high (400V). As a result, a high step-up converter is required to boost and regulate the low output voltage of fuel cell stacks in the fuel cell power system [2]. It allows to obtain a desired high DC voltage without having to increase the fuel cell stack size. Also, to ensure energy-efficient operation in fuel cell stacks, the output current ripple in fuel cell stacks should be considered. A large output current ripple causes the hydrogen utilization and fuel cell life time to be decreased. Therefore, a high step-up

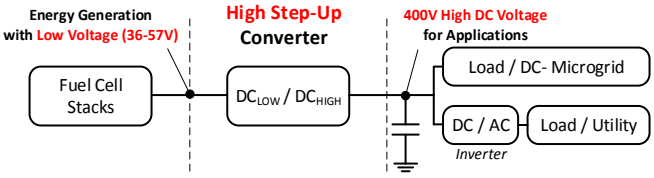

Fig. 1. Fuel cell power system with high step up converter.

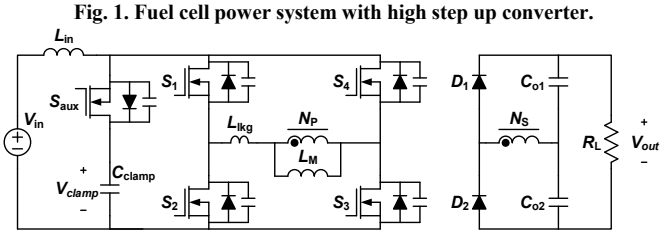

Fig. 2. Conventional active clamped current-fed full-bridge converter.

converter for fuel cell power system should have low input current ripple [3]. In low-input-voltage and high-output-voltage applications, an active clamped current-fed full-bridge (ACCF) converter is widely used because of its high step-up ratio, low input current ripple, and ZVS capability, as shown in Fig. 2. However, since large duty ratio *D* is used for high step-up ratio, the primary switch voltage stress influenced by *D* is high. In addition, the conduction loss of main switches S_1-S_4 is considerable due to a large peak current. Moreover, high turn-off current flows through the auxiliary switch S_{aux} generating large turn-off switching loss. In addition, since S_{aux} operates with doubled switching frequency, the turn-off loss is accelerated. These disadvantages decrease the efficiency of conventional ACCF converter [4, 5, 6]. In this paper, the half-bridge *LLC* converter is integrated to the conventional ACCF converter as shown in Fig. 3. Without additional active switches and volume increasing, the proposed converter enhances its efficiency by reducing the conduction and turn-off losses.

II. PROPOSED CONVERTER

The proposed converter is active clamped current-fed full-bridge converter integrating half-bridge *LLC* converter that consists of resonant capacitor C_r, leakage inductor L_{lkg2}, and magnetizing inductor L_{m2}. as shown in Fig. 3. No additional active component is required to integrate the half-bridge *LLC* converter. In addition, the proposed converter can be made without additional volume increasing. The output capacitors C_{o3} and C_{o4} for the *LLC* converter are stacked up in the second-

978-1-5090-1210-7/16/$31.00 ©2016 IEEE

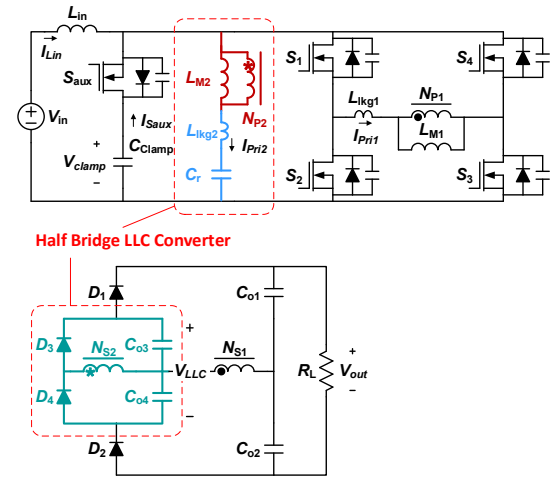

Fig. 3. Proposed active clamped current-fed full-bridge integrating *LLC* converter.

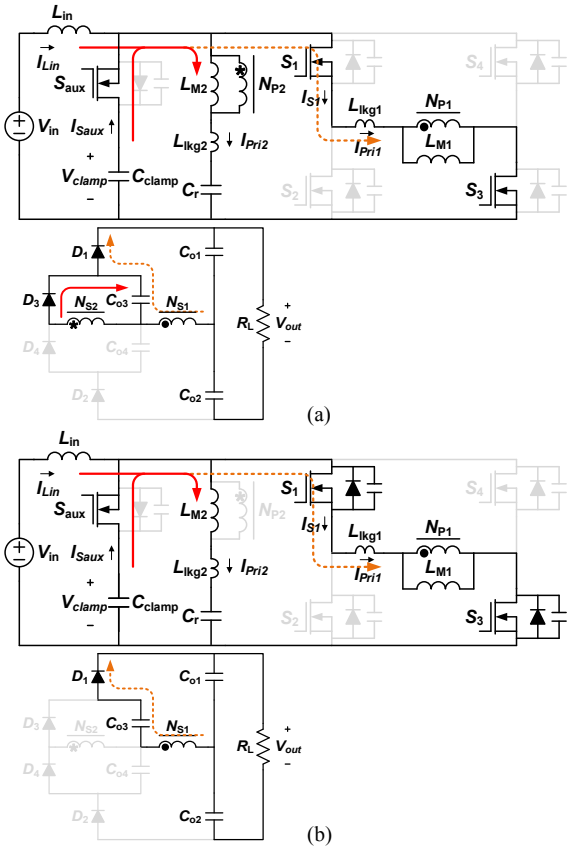

ary side. A small duty ratio D can be utilized in stacked-up output structure. As a result, the voltage stress of all switches is reduced owing to small D. Hence, the proposed converter employs low-voltage-rated switches with low $R_{DS(ON)}$. Moreover, the power is transferred to the load through two transformers which divide the powering current. Hence, the conduction loss of main switch S_1-S_4 is decreased by reducing the peak current. Furthermore, the turn-off current of auxiliary switch S_{aux} is decreased by sinusoidal shaped current of the *LLC* resonant tank, which results in small turn-off switching loss of S_{aux}. Similarly to the conventional ACCF converter, the ZVS operation of all switches is performed in the proposed converter.

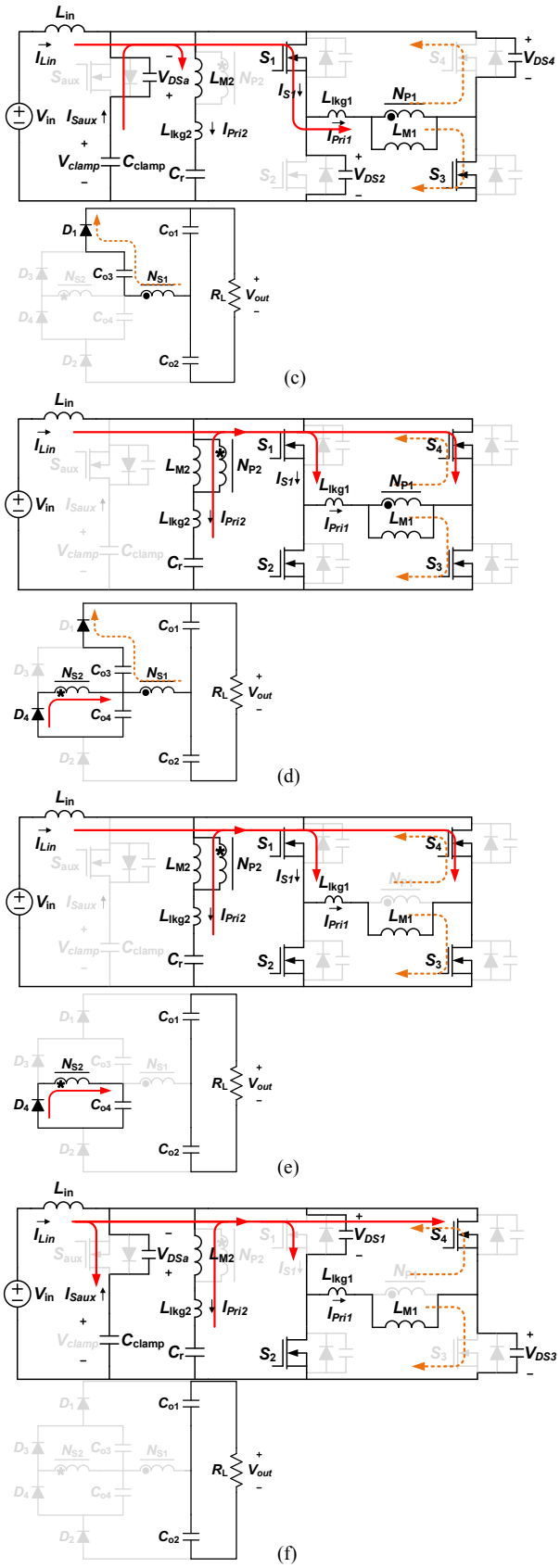

Fig. 4. Operational modes of proposed converter.
(a) $M_1[t_0$-$t_1]$, (b) $M_2[t_1$-$t_2]$, (c) $M_3[t_2$-$t_3]$, (d) $M_4[t_3$-$t_4]$, (e) $M_5[t_4$-$t_5]$, (f) $M_6[t_5$-$t_6]$

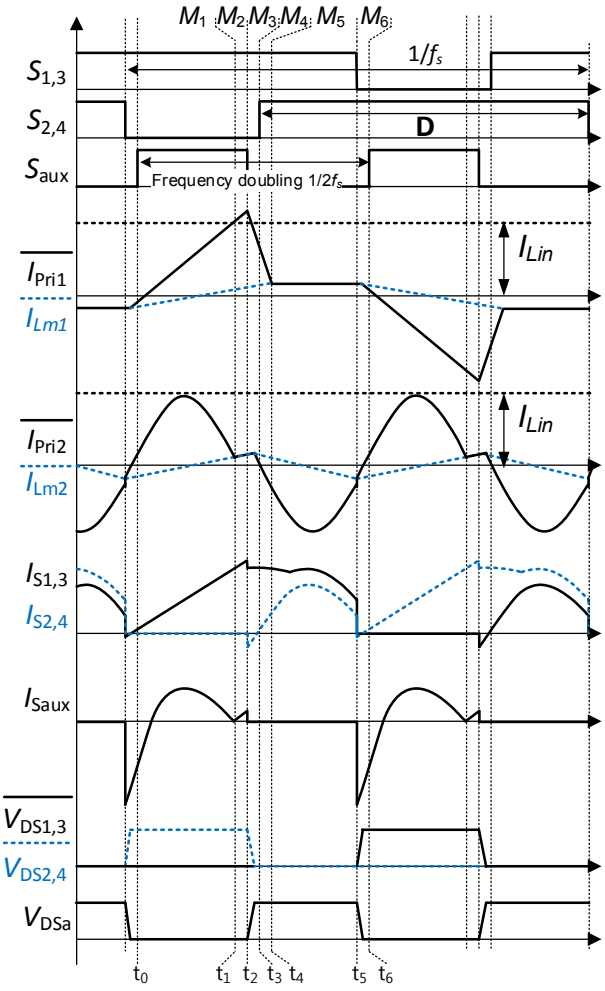

Fig. 5. Key waveforms of proposed converter.

A. Mode Anaylsis

The operations in the proposed converter are shown in Fig. 4. The operation can be divided into 6 modes by switching signals. The key waveforms are shown in Fig. 5. The switch S_1 and S_3 has the identical gating signal, and S_2 and S_4 has common gating signal. The gate signal of S_2 and S_4 is phase shifted by 180◦ with the gate signal of S_1 and S_3. The fixed frequency duty cycle modulation is used for the control. Two assumptions are made to understand the operation of the proposed converter. 1) The input inductor L_{in} is large so that input inductor current I_{Lin} is considered constant. 2) The clamp capacitor C_{clamp} is large so that clamp capacitor voltage V_{clamp} is constant.

***M1* [*t0-t1*] :** S_1, S_3 are ON. S_2 and S_4 are OFF. S_{aux} is turned on at t_0. C_{clamp} operates as voltage source for both converters. The primary current I_{Pri1} is increased by V_{clamp}, transferring the energy through output diode D_1. At the same time, L_{lkg2} resonates with C_r. The primary current I_{Pri2} transfers the energy through output diode D_3.

***M2* [*t1-t2*] :** I_{Pri2} and magnetizing inductor current I_{Lm2} are equal at t_1, and D_3 is turned off.

***M3* [*t2-t3*] :** S_{aux} is OFF at t_2. The current I_{ZVS1}, which is expressed as (1), discharges parasitic capacitor C_{oss1} of S_2 and S_4 and charges parasitic capacitor C_{oss2} of S_{aux}. The leakage inductor L_{lkg1} resonates with $2C_{oss1}$ and C_{oss2}. The equivalent circuit for the ZVS during M_3 is shown in Fig. 6.

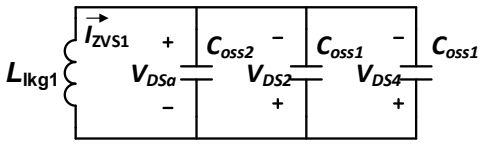

Fig. 6. Equivalent circuit during M_3.

$$I_{ZVS1} = I_{Pri1}(t_2) + I_{Pri2}(t_2) - I_{Lin} \quad (1)$$

ZVS condition

$$\frac{1}{2}L_{lkg1}I_{ZVS1}^2 \geq C_{oss1}V_{Clamp}^2 + \frac{1}{2}C_{oss2}V_{clamp}^2 \quad (2)$$

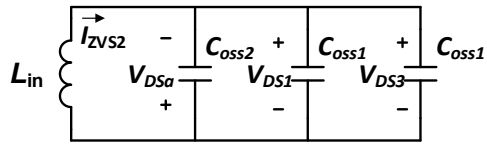

Fig. 7. Equivalent circuit during M_6.

$$I_{ZVS2} = I_{Lin} + I_{Pri1}(t_5) - I_{Pri2}(t_5) \quad (3)$$

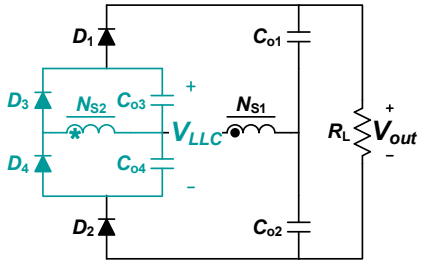

Fig. 8. Secondary Side Structure of Proposed Converter

$$V_{out,Prop} = V_{FB} + V_{LLC} = V_{out,Conv} + V_{LLC}$$

$$= \frac{2n_1V_{in}}{(1-D)A + \sqrt{(1-D)^2A^2 + 4An_1^2B}} + \frac{V_{in}n_2}{2(1-D)}\mathrm{M_{LLC}} \quad (4)$$

$$\left\{ A = \left(1 + \frac{1}{k}\right), B = \frac{2L_{lkg1}f_s}{R_L}, k = \frac{L_{m1}}{L_{lkg1}}, \right.$$
$$\left. n_1 = \frac{N_{S1}}{N_{P1}}, n_2 = \frac{N_{S2}}{N_{P2}}, M_{LLC} \cong 1 \right\}$$

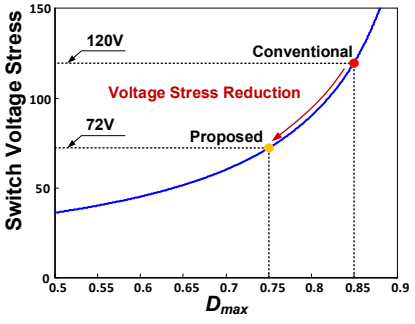

Fig. 9. Switch voltage stress with respect to Duty ratio

$$V_{DS,Switch} = V_{clamp} = \frac{V_{in,min}}{2(1-D_{max})} \quad (5)$$

***M4-M5* [*t3-t5*] :** S_2 and S_4 are turned on with the ZVS. All main switches S_1-S_4 are turned on during M_4-M_5. The input inductor current I_{Lin} is increased by the input voltage V_{in}. L_{lkg2} resonates with resonant capacitor C_r to opposite direction. I_{Pri2} transfers the energy through output diode D_4. M_4 and M_5 are

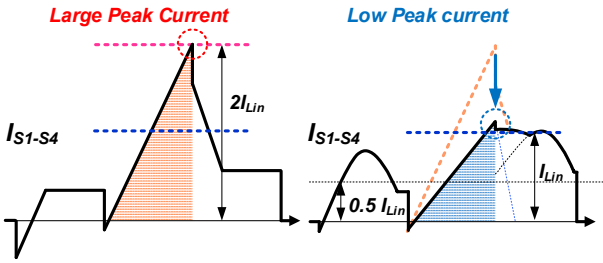

(a) Conventional (b)Proposed

Fig. 10. Main switch current waveform

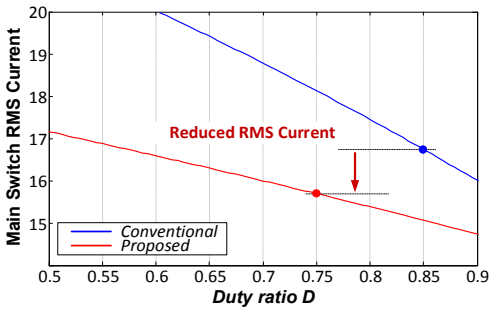

Fig. 11. Main switch RMS current

$$I_{S1,RMS,Conv} = I_{in}\sqrt{\frac{4(1-D)}{3}+\frac{2D-1}{4}} \quad (6)$$

$$I_{S1,RMS,Prop} = I_{in}\sqrt{\frac{1-D}{3}+\frac{1}{4}} \quad (7)$$

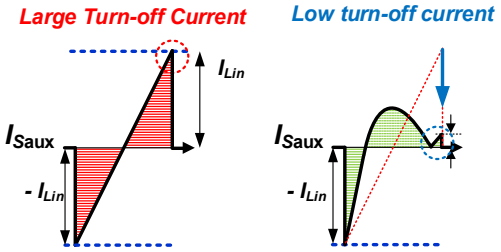

(a) Conventional (b)Proposed

Fig. 12. Auxiliary switch current waveform

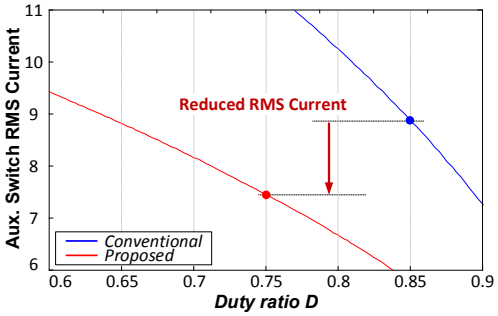

Fig. 13. Auxiliary switch RMS current

$$I_{Aux,RMS,Conv} = \sqrt{\frac{2}{T_s}\int_0^{(1-D)T_s}\left(I_{in}-\frac{2nI_{out}}{(1-D)^2T_s}t\right)^2 dt} \quad (8)$$

$$I_{Aux,RMS,Prop} = \sqrt{\frac{2}{T_s}\int_0^{(1-D)T_s}\left(I_{in}-\frac{2n_1I_{out}}{(1-D)^2T_s}t-\frac{\pi n_2 I_{out}}{(1-D)}sin\left(\frac{\pi}{(1-D)T_s}t\right)\right)^2 dt} \quad (9)$$

divided when D_1 is turned off at t_4.

M_6 [t_5-t_6] : S_1 and S_3 are turned off. I_{ZVS2}, which is expressed as (3), discharges parasitic capacitor C_{oss2} of S_{aux} and charges parasitic capacitor C_{oss1} of S_1 and S_3. The equivalent circuit for ZVS during M_6 is shown in Fig. 7. For the next half cycle, the operation is repeated in the same sequence with other symmetrical devices.

B. Feature of Proposed Converter

At the secondary side, output voltage of *LLC* part V_{LLC} is inserted in series at output voltage of full bridge part V_{FB} as shown in Fig.8. Final output voltage $V_{out,Prop}$ is sum of V_{FB} and V_{LLC} as (4). On the other hand, V_{FB} has a same form with the conventional ACCF converter output voltage $V_{out,Conv}$ due to same structure with the conventional ACCF converter. Therefore, the proposed converter has a higher voltage conversion gain with additional output voltage V_{LLC}. A high voltage conversion ratio can be achieved with a low duty ratio D. According to Fig. 9, voltage stress of all switches $V_{DS,Switch}$ is reduced. As a result, low-voltage-rated switches with low $R_{DS(ON)}$ can be chosen. By the voltage–sec balance of L_{in}, equation (5) can be obtained.

In case of the conventional ACCF converter, a large peak current flows on main switches S_1-S_4 as shown in Fig. 10(a). By the current-sec balance of C_{clamp}, the peak current of twice the average input current I_{Lin} is produced during C_{clamp} discharging period. Meanwhile, in case of the proposed converter, two transformers divides primary peak current half as shown in Fig. 10(b). And the RMS current of S_1-S_4 is reduced by decreased peak current as shown in Fig. 11. As a result, the conduction loss of S_1-S_4 is reduced. Each points on graph Fig.11. means design points of both converters.

For the conventional ACCF converter, a turn-off current on S_{aux} is large due to the current-sec balance of C_{clamp} as shown in Fig. 12(a). However, as shown in Fig. 12(b), the turn-off current on S_{aux} is reduced due to the sinusoidal shaped current of the *LLC* resonant tank. Also, a positive peak current is reduced. Therefore, RMS current of auxiliary switch S_{aux} is reduced as shown in Fig. 13. Each points on graph Fig. 13. means design points of both converters. Consequently, the turn-off loss and the conduction loss of auxiliary switch S_{aux} are significantly reduced.

III. Experimental Result

To verify effectiveness of proposed converter, a prototype converter has been implemented with following specification: Input voltage V_{in} varies from 36V to 57V depending on load condition. Rated output voltage V_{out} is 400V. Rated output power P_{out} is 1kW. Switching frequency of main switches f_s is 60kHz.

For the comparison, the prototype of the conventional ACCF converter has been implemented. The components of the conventional and the proposed converter are listed in Table. 1. Switches are selected as follow. In the proposed converter, IPP075N15N is used for S_1-S_4, and IRFI4510GPBF is used for S_{aux}. In the conventional converter, IRFP4668PBF is used for S_1-S_4, and IRFP250NPbF is used for S_{aux}. It is noticeable that

List of components	Conventional ACCF converter		Proposed converter
Main switches (S_1-S_4)	IRFP4668PbF (**200V**/130A)		IPP07515N3G (**150V**/100A)
Auxiliary switch (S_{aux})	IRFP250N (**200V**/30A)		IRFI4510GPBF (**100V**/35A)
Output diodes	D_{O1}-D_{O2} : FFH50US60S (600V/50A)		D_{O1}-D_{O4} : 30EPH03 (300V/30A)
Input inductor	Core	**CH468060**	**CH400060**
	L_{in}	76μH	54μH
Transformer1	Core	PQ3535S	PQ3230S
	Turn ratio	6:15 (N_p:N_s)	7:14 (N_{P1}:N_{S1})
	L_{m1}	168μH	212μH
	L_{lkg1}	1.34μH	2.92μH
Transformer2	Core	-	PQ3220S
	Turn ratio	-	4:11 (N_{P2}:N_{S2})
	L_{m2}	-	32μH
	L_{lkg2}	-	0.4μH
Output capacitor	C_{O1}-C_{O2}	250V,560μF (6ea)	250V, 560μH (4ea)
	C_{O3}-C_{O4}	-	160V, 330μH (8ea)
Clamp capacitor	C_{clamp}	160V,330μF (7ea)	100V,220μF (8ea)
Resonant capacitor	C_r	-	250V, 4.4μF

Table. 1. List of components.

List of components	Conventional ACCF converter	Proposed converter	
Output diode	18.4cm^3 (D_{O1}-D_{O2})	36.8cm^3 (D_{O1}-D_{O4})	+18.4cm^3
Input inductor	59.11cm^3 (CH468060)	47.12cm^3 (CH400060)	-11.99cm^3
Transformers	31.71cm^3 (PQ3535S)	35.83 cm^3 (PQ3230S, PQ3220S)	+4.12cm^3
Output capacitor	148.44cm^3 (C_{O1}-C_{O2})	163.08cm^3(C_{O1}-C_{O2}, C_{O3}-C_{O4})	
Clamp capacitor	56.11cm^3 (C_{clamp})	25.54cm^3 (C_{clamp})	
Resonant capacitor	-	7.5cm^3 (C_r)	
Capacitor total	204.55cm^3	195.13cm^3	-9.42cm^3
Total volume	**313.78cm^3**	**314.88cm^3**	**+1.1cm^3**

Table. 2. Volume comparison of converters.

the volume of major components for the proposed converter is 314.88cm^3. And the volume of major components for the conventional converter is 313.78cm^3. Although the volume of transformer is increased, the volume of input inductor and clamp capacitor are decreased. Consequently, total volume of the proposed converter is barely increased as shown in Table. 2. Fig. 14. shows the key experimental waveforms of the

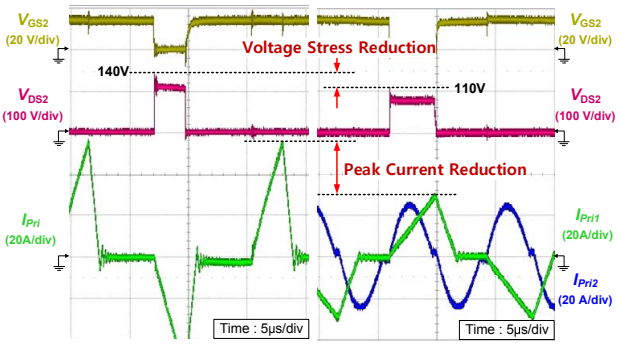

(a) Conventional (b)Proposed

Fig. 14. Switch voltage stress and Transformer primary current. (full load condition)

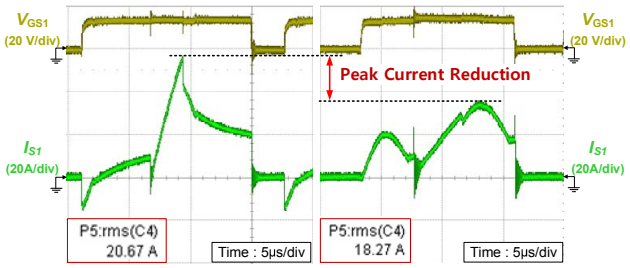

(a) Conventional (b)Proposed

Fig. 15. Main switch S_1 current waveform.

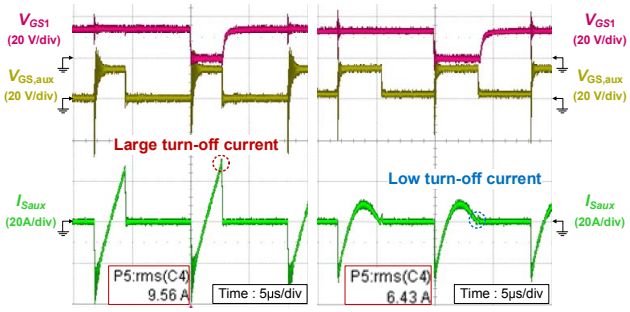

(a) Conventional (b)Proposed

Fig. 16. Auxiliary switch S_{aux} current waveform.

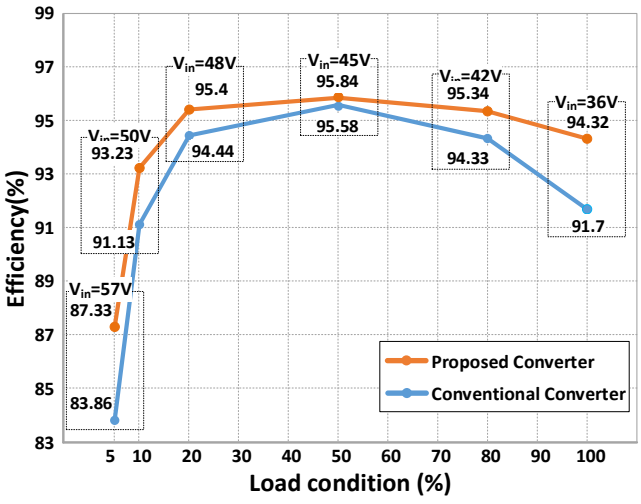

Fig. 17. Efficiency curve.

proposed converter at full load condition. Switch voltage stress is reduced owing to low duty ratio D as shown in Fig. 14. In addition, since the power is transferred to the load through

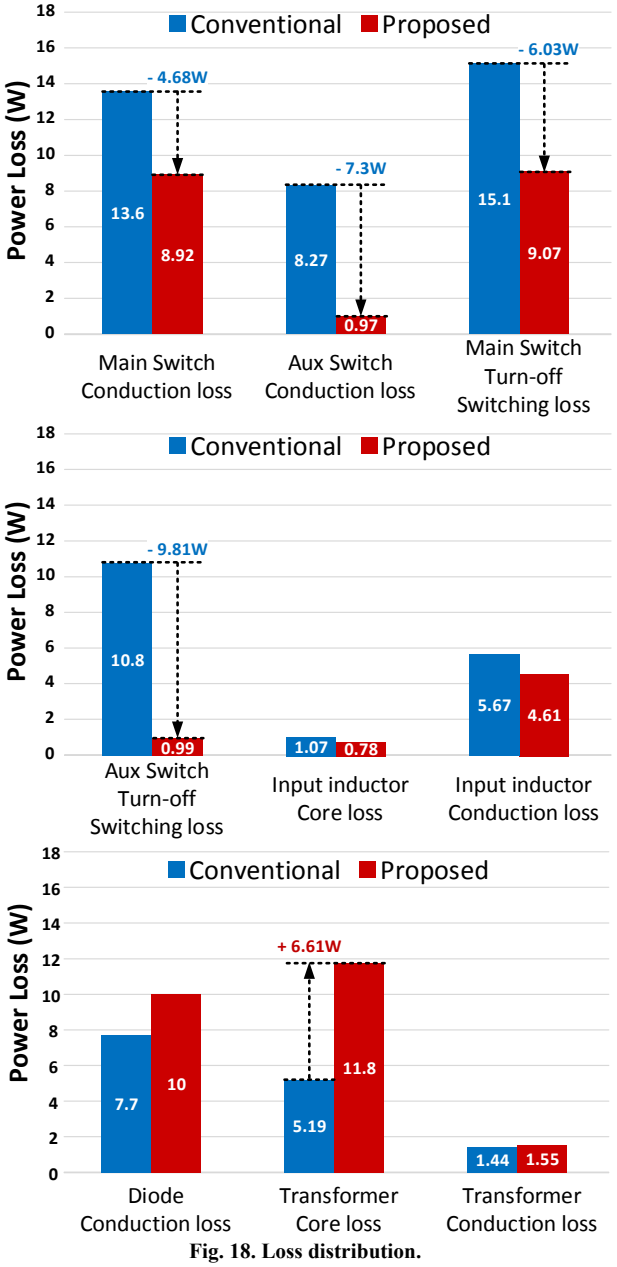

Fig. 18. Loss distribution.

two transformers, transformer primary peak current is reduced. As a result, the conduction loss of S_1-S_4 is reduced with low RMS current value as shown in Fig. 15. The turn-off switching loss of S_{aux} is decreased by sinusoidal resonant current as shown in Fig. 16. The conduction loss of S_{aux} is also decreased with low RMS current value. The efficiency of proposed converter is 94.32% at the full load. The efficiency of conventional converter is 91.7% at the full load. The proposed converter enhances the efficiency at the entire load condition as shown in Fig. 17. The efficiency is measured at each load condition varying the input voltage.

The loss distribution of the conventional ACCF converter and proposed converter are shown in Fig. 18. In case of the proposed converter, since the peak current of main switches is reduced and low-voltage-rated switches are employed with low $R_{DS(on)}$, conduction loss of four main switches S_1-S_4 is reduced. Moreover, turn off switching loss of main switches is also reduced due to small overlap area resulting from low voltage stress. The conduction loss of auxiliary switch S_{aux} is considerably reduced because of low RMS current and low $R_{DS(on)}$ resulting from low voltage stress. By sinusoidal resonant waveform of *LLC* resonant tank resulting in low turn-off current on S_{aux}, turn-off switching loss of S_{aux} is significantly reduced. On the other hand, because transformer for *LLC* converter is operated with $2f_s$ = 120kHz, transformer core loss is increased. Consequently, the proposed converter has higher efficiency compared to conventional ACCF converters.

IV. Conclusion

In this paper, active clamped current-fed full-bridge converter integrating the *LLC* converter is proposed for interfacing the fuel cell stacks. The half-bridge *LLC* converter is integrated without additional active component and volume increasing. In the proposed converter, all advantages results from the power distribution using two transformers. The voltage stress of the primary switches is reduced by small duty ratio D resulting from its high step-up ratio. Therefore, the primary switches with low $R_{DS(on)}$ can be chosen. Furthermore, the conduction loss of S_1-S_4 is reduced due to the low peak current, and the turn-off switching loss of S_{aux} is reduced by the low turn-off current. The conduction loss of S_{aux} is also reduced by low positive peak current. Experimental results with 1kW prototype show that the proposed converter has higher efficiency compared with the conventional converter. Consequently, the proposed converter is expected to be suitable at fuel cell power system with high efficiency.

Acknowledgment

This work was supported by the National Research Foundation of Korea(NRF) grant funded by the Korea government (MSIP) (No. 2010-0028680).

References

[1] J. Larminie and A. Dicks, "Fuel Cell Systems Explained." New York: Wiley, 2002.

[2] K.-C. Tseng, J.-T. Lin, and C.-C. Huang, "High Step-Up Converter With Three-Winding Coupled Inductor for Fuel Cell Energy Source Applications," *IEEE Trans. Power Electron.*, vol. 30, no. 2, pp. 574–581, Feb. 2015.

[3] S. K. Mazumder, R. K. Burra, and K. Acharya, "A Ripple-Mitigating and Energy-Efficient Fuel Cell Power-Conditioning System," *IEEE Trans. Power Electron.*, vol. 22, no. 4, pp. 1437–1452, Jul. 2007.

[4] U. R. Prasanna, and A. K. Rathore, "Extended Range ZVS Active-Clamped Current-Fed Full-Bridge Isolated DC / DC Converter for Fuel Cell Applications : Analysis , Design , and Experimental Results," *IEEE Trans. Ind. Electron.*, vol. 60, no. 7, pp. 2661–2672, Jul. 2013.

[5] M. Nymand, and M. A. E. Andersen, "High-efficiency isolated boost DC/DC converter for high-power low-voltage fuel-cell applications," *IEEE Trans. Ind. Electron.*, vol. 57, no. 2, pp. 505–514, Feb. 2010.

[6] A. Mousavi, , P. Das, and G. Moschopoulos, "A Comparative Study of a New ZCS DC–DC Full-Bridge Boost Converter With a ZVS Active-Clamp Converter" *IEEE Trans. Power Electron.,* vol. 27, no. 3, pp. 1347–1358, Mar. 2012.

[7] S. J. Cheng, Y. K. Lo, H. J. Chiu, and S. W. Kuo, "High-efficiency digital-controlled interleaved power converter for high-power PEM fuel-cell applications," *IEEE Trans. Ind. Electron.*, vol. 60, no. 2, pp. 773–780, Feb. 2013.

[8] X. Kong and A. M. Khambadkone, "Analysis and implementation of a high efficiency, interleaved current-fed full bridge converter for fuel cell system," *IEEE Trans. Power Electron.*, vol. 22, no. 2, pp. 543–550, Mar. 2007.

[9] K.-C. Tseng, C.-C. Huang, and C.-A. Cheng, "A High Step-Up Converter with Voltage-Multiplier Modules for Sustainable Energy Applications," *IEEE J. Emerg. Sel. Top. Power Electron.*, vol. 3, no. 4, pp. 1100–1108, Dec. 2015.

[10] B. Yuan, X. Yang, X. Zeng, J. Duan, J. Zhai, and D. Li, "Analysis and design of a high step-up current-fed multiresonant DC-DC converter with low circulating energy and zero-current switching for all active switches," *IEEE Trans. Ind. Electron.*, vol. 59, no. 2, pp. 964–978, Feb. 2012.

[11] A. Averberg, K. R. Meyer, and a. Mertens, "Current-fed full bridge converter for fuel cell systems," *PESC Rec. - IEEE Annu. Power Electron. Spec. Conf.*, pp. 866–872, 2008.

[12] O. a Ahmed and J. Bleijs, "Optimized active-clamp circuit design for an isolated full-bridge current-fed DC-DC converter," in *2011 4th International Conference on Power Electronics Systems and Applications*, 2011.

[13] U. R. Prasanna, P. Xuewei, A. Rathore, and K. Rajashekara, "Propulsion system architecture and power conditioning topologies for fuel cell vehicles," *IEEE Trans. Industry applications.*, vol. 51, no. 1, pp. 640–650, Jan/Feb. 2015.

[14] U. R. Prasanna and A. K. Rathore, "Analysis and design of zero-voltage-switching current-fed isolated full-bridge Dc/Dc converter," *Proc. Int. Conf. Power Electron. Drive Syst.*, no. December, pp. 239–245, 2011.

[15] V. Yakushev, V. Meleshin, and S. Fraidlin, "Full-bridge isolated current fed converter with active clamp," *APEC '99. Fourteenth Annu. Appl. Power Electron. Conf. Expo. 1999 Conf. Proc.*, vol. 1, 1999.

[16] S. K. Han, H. K. Yoon, G. W. Moon, M. J. Youn, Y. H. Kim, and K. H. Lee, "A new active clamping zero-voltage switching PWM current-fed half-bridge converter," *IEEE Trans. Power Electron.*, vol. 20, no. 6, pp. 1271–1279, Nov. 2005.

[17] J. M. Kwon, E. H. Kim, B. H. Kwon, and K. H. Nam, "High-efficiency fuel cell power conditioning system with input current ripple reduction," *IEEE Trans. Ind. Electron.*, vol. 56, no. 3, pp. 826–834, Mar. 2009.

[18] K. R. Sree, A. K. Rathore, E. Breaz, and F. Gao, "Soft switching Non-isolated Current-fed Inverter for PV/Fuel Cell Applications," *IEEE Trans. Industry applications.*, vol. 52, no. 1, pp. 351–359, Jan/Feb. 2016.

[19] G. Fontes, C. Turpin, S. Astier, and T. A. Meynard, "Interactions Between Fuel Cells and Power Converters: Influence of Current Harmonics on a Fuel Cell Stack," *IEEE Trans. Power Electron.*, vol. 22, no. 2, pp. 670–678, Mar. 2007.

[20] L. Zhang, D. Xu, G. Shen, M. Chen, A. Ioinovici, and X. Wu, "A High Step-Up DC to DC Converter under APS Control for Fuel Cell Power System," *IEEE Trans. Power Electron.*, vol. 30, no. 3, , pp. 1694–1703, Mar. 2014.

[21] C. T. Pan and C. M. Lai, "A high-efficiency high step-up converter with low switch voltage stress for fuel-cell system applications," *IEEE Trans. Ind. Electron.*, vol. 57, no. 6, pp. 1998–2006, Jun. 2010.

[22] A. Shahin, M. Hinaje, J. P. Martin, S. Pierfederici, S. Rael, and B. Davat, "High voltage ratio DC-DC converter for fuel-cell applications," *IEEE Trans. Ind. Electron.*, vol. 57, no. 12, pp. 3944–3955, Dec. 2010.